Paleoceanography and Paleoclimatology

RESEARCH ARTICLE
10.1029/2023PA004739

Key Points:

- Ice ages may either be driven by insolation variations or represent self-sustained oscillations merely paced by the variations in insolation
- We propose analyses to produce observable differences between these two scenarios and demonstrate them using two simple models
- For the example models, the results suggest that ice ages are self-sustained oscillations paced by insolation rather than driven

Supporting Information:

Supporting Information may be found in the online version of this article.

Correspondence to:

K. Koepnick,
kirstinkoepnick@g.harvard.edu

Citation:

Koepnick, K., & Tziperman, E. (2024). Distinguishing between insolation-driven and phase-locked 100-Kyr ice age scenarios using example models. *Paleoceanography and Paleoclimatology*, *39*, e2023PA004739. https://doi.org/10.1029/2023PA004739

Received 8 AUG 2023
Accepted 6 MAR 2024

Distinguishing Between Insolation-Driven and Phase-Locked 100-Kyr Ice Age Scenarios Using Example Models

Kirstin Koepnick[1] **and Eli Tziperman**[1,2]

[1]School of Engineering and Applied Sciences, Harvard University, Cambridge, MA, USA, [2]Department of Earth and Planetary Sciences, Harvard University, Cambridge, MA, USA

Abstract Glacial-interglacial oscillations exhibit a periodicity of approximately 100 Kyr during the late Pleistocene. Insolation variations are understood to play a vital role in these ice ages, yet their exact effect is still unknown; the 100 Kyr ice ages may be explained in two different ways. They could be purely insolation-driven, such that ice ages are a consequence of insolation variations and would not have existed without these variations. Or, ice ages may be self-sustained oscillations, where they would have existed even without insolation variations. We develop several observable measures that are used to differentiate between the two scenarios and can help to determine which one is more likely based on the observed proxy record. We demonstrate these analyses using two representative models. First, we find that the self-sustained model best fits the ice volume proxy record for the full 800-Kyr time period. Next, the same model also shows a 100 Kyr peak consistent with observations, yet the insolation-driven model exhibits a dominant 400 Kyr spectral peak inconsistent with observations. Our third measure indicates that midpoints in ice volume during terminations do not always occur during the same phase of insolation in both observations and the self-sustained scenario, whereas they do in the insolation-driven scenario. While some of these results suggest that the self-sustained ice ages are more consistent with the observed record, they rely on simple representations of the two scenarios. To draw robust conclusions, a broader class of models should be tested using this method of producing observable differences.

1. Introduction

Over the past 800,000 years, climate has been dominated by saw-tooth-like glacial oscillations with a periodicity of about 100,000 years. The driving force behind these oscillations, the cause of the saw-tooth structure, the periodicity of 100 kiloyears (Kyr), and the reason for and role of CO_2 changes are still not well understood. Although it is broadly accepted that Earth's orbital variations play a role in these cycles, the precise extent and mechanism of influence of these variations on the ice sheets' evolution is still unclear. Due to the variations in orbital parameters (eccentricity, obliquity, and precession), the insolation variation is characterized by approximately 20, 40, and 100 Kyr cycles. Although there is a 100 Kyr periodicity in the incoming solar radiation due to variations in Earth's orbital eccentricity, the amplitude of this signal is quite small, while the 100 Kyr cycle dominates the ice volume records. This seeming mismatch is commonly referred to as the Milankovitch paradox or the 100 Kyr problem (Hays et al., 1976; Imbrie, Mix, & Martinson, 1993; Paillard, 2001).

Proposed mechanisms for the role of Milankovitch forcing can be divided into two different classes, describing the glacial oscillation either as an oscillation driven by the variations in insolation that would not have existed if insolation were constant (we refer to this as the first scenario or as the insolation-driven oscillations). Alternatively, the ice ages may be seen as a "self-sustained" oscillation that is driven by internal climatic feedbacks and that would have existed even without orbital variations, possibly with somewhat different periodicity and different termination times than observed (second scenario). In this second scenario, orbital variations determine the phase of the oscillations, as expressed by the time of terminations, but are not responsible for their existence. In this scenario, Milankovitch forcing thus acts as a "pacemaker" of the glacial cycles, in the spirit of Hays et al. (1976). This convergence of glacial cycles to the observed record due to the insolation variations is referred to as nonlinear phase locking or synchronization. We define internally driven/self-sustained glacial cycles by the existence of an oscillation even without Milankovitch forcing. We consider phase locking to be relevant to an oscillating dynamical system that is self-sustained, following Pikovsky et al. (2001), although there can be other definitions. Figuring out which of these two scenarios is more plausible would be a significant step toward an improved understanding of ice ages and is the motivation of this study.

Example glacial models of the first scenario (insolation-driven oscillations) include, for example, Weertman (1976), Imbrie and Imbrie (1980), Paillard (1998) and the recent Abe-Ouchi et al. (2013, hereafter AO2013). Example mechanisms and glacial models that follow the second scenario (self-sustained oscillations phase-locked to Milankovitch forcing) are Ghil and Saltzman (1984), Maasch and Saltzman (1990), Hyde and Peltier (1987), De Saedeleer et al. (2013), Crucifix (2013), and the sea-ice switch model (Gildor & Tziperman, 2000; Tziperman et al., 2006). It is not always clear into which scenario published models fall (e.g., Ganopolski & Brovkin, 2017; Pollard, 1982; Willeit et al., 2019) as the classification sometimes requires further analysis that was not the focus of a given paper.

In this paper, we develop a series of analyses to distinguish between these two alternative scenarios using two simple models and the comparison to observations. The use of simple models allows us to perform mechanism denial experiments and parameter sensitivity tests and examine the tolerance to noise, which are all not possible with a comprehensive climate model. To study the insolation-driven ice ages scenario, we create a simple model based on the work of AO2013, while to describe a phase-locked self-sustained glacial oscillation scenario, we use a modified version of the sea ice switch (SIS) model (Gildor & Tziperman, 2000; Tziperman et al., 2006). We use these simple models to showcase our approach to producing observable differences. This approach could be combined with a broader set of models and data sets to draw more robust conclusions than are possible here.

To identify observable differences between the two scenarios, we use the benthic δ^{18}O stack of Lisiecki (2010) as a proxy for ice volume, although the benthic δ^{18}O encodes both land ice volume and benthic temperature (Adkins & Schrag, 2001; Emiliani, 1955; Epstein et al., 1953; Shackleton, 1967). This stack takes the same benthic stack as Lisiecki and Raymo (2005) and assigns a non-orbitally tuned age model assuming a constant sedimentation rate. The deep ocean temperature contribution was estimated to be about half the δ^{18}O signal for the Last Glacial Maximum (LGM) (Adkins & Schrag, 2001). Spratt and Lisiecki (2016) produced a sea level stack for the last 800 Kyr by removing the temperature contribution using the temperature-dependent fractionation effect and using orbital tuning. The tunning makes the resulting record less appropriate for our purposes, as one of our objectives is to examine the phase relationship between Milankovitch forcing and terminations.

In the following, we first describe the data and proxy records used as observations in Section 2.1. Then we discuss the formulation of our simple model of insolation-driven ice ages (the insolation-driven simple model, hereafter the IDSM, in Section 2.2) and a modified version of the SIS model (Section 2.3). Our results in Section 3 are broken into an exploration of several issues: the fit to proxy records (Section 3.1), the phase of Milankovitch forcing during terminations (Section 3.2), the relationship between termination-integrated insolation and ice volume drop during terminations (Section 3.3) the sensitivity to initial conditions (Section 3.4), and then the effects of and sensitivity to noise (Section 3.5). Finally, we conclude with a discussion in Section 4.

2. Methods: Models and Data

In this section, we discuss the proxy records used and present the insolation-driven simple model we developed following AO2013 as well as a modified version of the SIS model we created based on Gildor and Tziperman (2000) and Tziperman et al. (2006).

2.1. Data

We use the insolation forcing for June 21st at 65°N calculated by Berger (1978). Since the difference between Berger (1978) and Berger and Loutre (1991) is minor over the last 800 Kyr, we proceed with Berger (1978) to be consistent with Tziperman et al. (2006). Many different measures of insolation have been proposed to play a role in ice ages. An integrated insolation above some prescribed threshold was suggested by Huybers (2006) to explain the 41-Kyr cycles. If the 100-Kyr oscillations occurred during an overall cooler climate, they may be better explained with a higher insolation threshold, where the integrated insolation is effectively equivalent to using the June 21st value. Insolation integrated over the caloric summer half of the year was used by some studies (Mitsui et al., 2022; Tzedakis et al., 2017). Similarly, Roe (2006) found a relationship between global ice volume rate of change, dV/dt, and the June 21st summer insolation. Clearly, forcing the models examined here with different insolation measures may lead to different results. It is not obvious apriori which one might be best, leading us to use the simple measure of June 21st insolation.

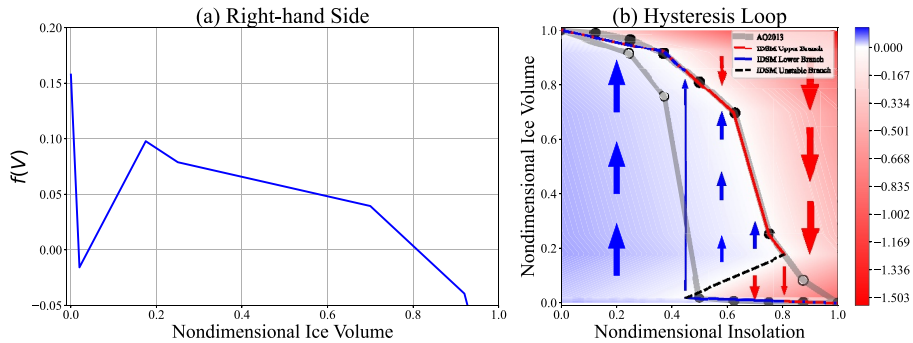

Figure 1. A simple model reproducing the results of AO2013. (a) The prescribed piecewise linear function $f(V)$ from Equation 1 which leads to the hysteresis loop in panel (b). (b) The hysteresis loop. The stable upper branch is shown by the red solid line, and the stable lower branch in solid blue. The unstable branch is indicated by the dashed black line. The background colors indicate the sign of dV/dt at each value of the insolation and ice volume, following AO2013. The red shading indicated a negative mass balance and the ablation of ice sheets, whereas the blue corresponds to a positive mass balance or accumulation of ice volume. The gray line shows AO2013's hysteresis curve for comparison; see text for details. The red and blue arrows correspond to the direction of the expected change in ice volume for different insolation and ice volume values. The python functions used to create this simple model are available through Koepnick (2024).

Global ice volume change is represented here by the oxygen isotope ratio, $\delta^{18}O$, in benthic foraminifera found in marine sediment cores. We use the $\delta^{18}O$-based reconstruction of Lisiecki (2010, hereafter LR04 untuned) that is not orbitally-tuned. This stack takes the same benthic stack as Lisiecki and Raymo (2005) and assigns a non-orbitally tuned age model assuming a constant sedimentation rate. We chose this reconstruction because it does not involve orbital tuning to Milankovitch forcing, as one of our goals is to test the models' predictions of the phase between the Milankovitch cycles and ice age termination or peak times. In our analysis, we define termination 6 (hereafter T6 and similarly for the other terminations) to be split into two steps: T6b (540–529 ka) and T6a (518–496 ka), motivated by the work of Spratt and Lisiecki (2016) who suggested that the first state is mostly temperature dominated while the second reflects ice volume changes.

We analyzed the 400 Kyr ice volume time series from AO2013 by digitizing their results (using Rohatgi, 2022) in order to compare the skill of our IDSM at replicating AO2013 before using the IDSM to explore the insolation-driven scenario.

For the spectral analysis shown in Section 3.1, we first linearly detrend the data. Then the power spectrum and associated 95% uncertainty range are computed using the multi-taper method with adaptive weighting (Donald & Percival, 1993; Huybers, 2022; Thomson, 1982). We also use Savitzky-Golay smoothing (python package `scipy.signal.savgol`) on the proxy record for plotting Figure 4 to make it more legible, using a window length of 9, and a polynomial order of 1. See supplementary material for the effects of smoothing (Figure S2 in Supporting Information S1).

2.2. Insolation-Driven Glacial Cycles: A Simplified Model of the AO2013 Mechanism

AO2013 used an ice sheet model driven by parameterized atmospheric feedback developed from a suite of general circulation model experiments (Abe-Ouchi et al., 2007) using the MIROC model (K-1 model developers, 2004). They find multiple ice sheet equilibria for a range of time-independent prescribed insolation amplitudes. Starting with either no ice volume or large ice volume, their model converges to two different steady states shown by the upper and lower gray dots and circles in Figure 1b. Because the model converges to a steady state with prescribed fixed insolation rather than developing ice age oscillations, while it develops glacial oscillations when Milankovitch variations in insolation are introduced, it represents the insolation-driven ice age scenario. The existence of multiple equilibria implies a hysteresis loop in the value of insolation over the range for which multiple equilibria are found: if the insolation is very slowly increased and then decreased, such that the ice volume is always in equilibrium with the insolation forcing, the volume is different in the increasing versus decreasing paths for any insolation amplitude in the range of multiple equilibria, as shown by the solid red and dashed blue curves of Figure 1b.

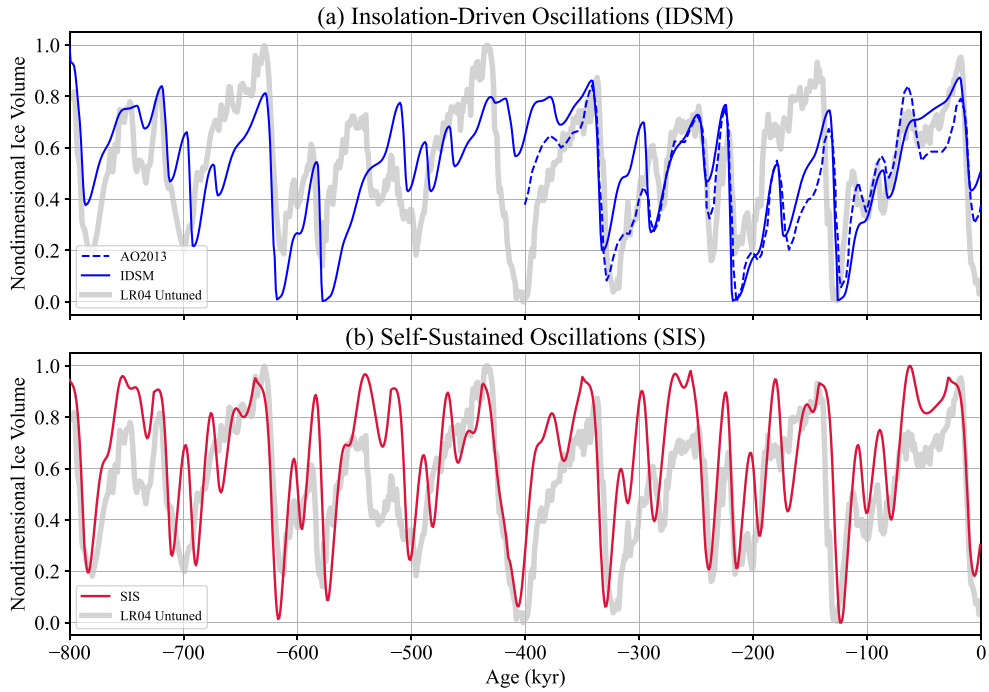

Figure 2. Overall fit of both scenarios to proxy record. (a) A time series for the insolation-driven simple model in blue and AO2013's results in dashed blue, both superimposed on observations (LR04 untuned). (b) Modified sea ice switch time series plotted in red against observations (Lisiecki, 2010) in thick gray.

We note that a hysteresis loop driven by multiple equilibria (two back-to-back saddle-node bifurcations, e.g., Sections 3.1 and 7.5 of Strogatz, 1994) involves an unstable branch and two abrupt jumps of ice volume as a function of insolation. It is not completely clear where the two jumps are in the AO2013 results, and the loop indicated by their Figure 2b, therefore, seems inconsistent with a standard hysteresis loop. We, therefore, took the liberty of assuming that the three AO2013 equilibrium points indicated in the figure by empty circles have perhaps not converged completely in their complex model simulations and should have led to the same ice volume value at a steady state as the full circles shown for the same insolation forcing amplitudes. This results in the hysteresis shape shown by the thin blue and red arrows in Figure 1b marking the presumed jump locations. We tested various locations of the jump locations and found the shown hysteresis loop resulted in the best match to the ice volume time series results of AO2013. We also show the implied location of the unstable solution expected in such a system (dashed black line). This unstable branch connects the last point of stability in the upper branch and the lower branch (Strogatz, 1994). Our red and blue background colors indicate the negative and positive values of the right-hand side (RHS) of the ice volume equation calculated by our model below, following AO2013. Unlike in AO2013, these colors also fill the area inside the hysteresis curve, allowing a detailed interpretation later in the paper.

AO2013 showed that when forced with a time variable Milankovitch forcing, this hysteresis loop leads to observed-like 100 Kyr oscillations, also roughly reproducing the observed timings of the glacial terminations even when holding CO_2 constant. Since including the observed CO_2 forcing would introduce an explicit 100 Kyr timescale and influence the timings of terminations, we only consider the AO2013 runs when holding CO_2 constant. As explained by AO2013, when including CO_2, ice ages were amplified, but the termination times were roughly the same. To allow performing various analyses and sensitivity experiments with this proposed mechanism, we create a simple model reproducing the results of the AO2013 mechanism under constant CO_2.

We only consider AO2013's North American ice sheet hysteresis and create a nonlinear ordinary differential equation (ODE) with a matching prescribed hysteresis loop. To begin, we consider a non-dimensional ice volume (V) equation of the form $dV/dt = f(V)$ where $V = 0$ indicates no ice volume and $V = 1$ denotes the maximal ice volume. We construct a piecewise linear function $f(V)$ (Figure 1a) that leads to the desired bistability as seen in Figure 1b. The hysteresis loop exactly matches the one found by the IcIES-MIROC model in AO2013 (noting our

above-mentioned minor modification of their results to make the hysteresis loop consistent with what one expects mathematically).

Our full nonlinear ODE based on the AO2013 results, which we refer to as the insolation-driven hysteresis simple model, or IDSM, is given by,

$$\frac{dV}{dt} = \beta f(V) - \gamma\left(I(t) - \frac{1}{2} + \nu_0\nu(t)\right); \qquad \beta = \begin{cases} 5\times10^{-8} & \text{if } f(V)<0, \\ \frac{1}{6}\times10^{-8} & \text{if } f(V)>0. \end{cases} \tag{1}$$

All variables are nondimensional except for time, which is measured in Kyr. The function $I(t)$ is June 21st insolation at 65°N (Berger, 1978), rescaled to vary between 0 and 1. The parameter $\gamma = 9\times10^{-8}$ Kyr^{-1} sets the amplitude of the solar forcing term in the surface mass balance of the ice sheet. The function $f(V)$ on the RHS, is our nondimensional piece-wise linear function shown in Figure 1a. To induce the expected slow growth and rapid melting, we introduce a scale, β Kyr^{-1}, which strengthens the negative mass balance and weakens the positive pull. Although ice growth is slow over long periods of time (e.g., 90 Kyr average), ice volume actually varies in a sequence of rapid increases and decreases (Broecker & van Donk, 1970). We do not attempt to model these rapid steps, including millennial-scale variability, although it has been suggested that they may be an important part of the dynamics (Barker & Knorr, 2021).

We introduce an optional stochastic (noise) forcing through the term $\nu_0\nu(t)$ in Equation 1. The stochastic forcing is a Markov process with an amplitude ν_0 in Equation 1, and with,

$$\nu(t_n) = R\nu(t_{n-1}) + \theta(t_n)\sqrt{1-R^2}. \tag{2}$$

Here, $R = \exp(-\Delta t/3\text{Kyr})$, $\Delta t = 1$ Kyr, and $\theta(t_n)$ describes a white Gaussian noise with a zero mean such that $\langle\theta_n\theta_m\rangle = 0.042\delta_{nm}$, and δ_{nm} denotes the Kronecker delta. A similar noise term was used by Tziperman et al. (2006).

The IDSM has three explicit tunable parameters (two values of β and γ), as well as the additional seven points used to construct the shape of the hysteresis curve, each specified by two parameters of insolation and ice volume (plus three more for the stochastic forcing term, when included). The IDSM has, therefore, 17 tunable parameters, which were adjusted to fit the last 400 Kyr results of AO2013. We use the IDSM given in Equation 1 to represent the insolation-driven ice age of the first scenario.

2.3. Internally Driven/Self-Sustained Glacial Cycles: A Modified Sea Ice Switch Model

We use a modified version of the SIS mechanism (Gildor & Tziperman, 2000; Tziperman et al., 2006) to represent self-sustained ice ages of the second scenario. The simplified SIS model is used here because it combines several elements useful for this study: First, it represents a self-sustained mechanism (setting Milankovitch forcing to a constant, still results in ice ages, see Figure S3c in Supporting Information S1). Second, it is a falsifiable mechanism in the sense that future proxy observations of sea ice during ice ages may prove it wrong, which is not the case for many idealized glacial models. Finally, its formulation is simple and easily reproducible.

The equation for the ice volume in the version of the SIS model used here (Tziperman et al., 2006) is,

$$\frac{dV}{dt} = \left(p_0 - kV\right)(1-a_{si}) - [S_0 + S_M I_{\text{trunc}}(t) + \nu_0\nu(t))], \tag{3}$$

where p_0 denotes the snow (ice) accumulation rate when the ice sheets and sea ice are entirely melted, k represents the elevation desert effect by which accumulation decreases with ice sheet volume (and height) so that the accumulation in the absence of sea ice is $p_0 - kV$. The parameter a_{si} is the nondimensional area fraction covered by sea ice: when sea ice is "off," $a_{si} = 0$, and otherwise, it is set to another constant value $\bar{a}_{si} > 0$. $I_{\text{trunc}}(t)$ is based on the June 21st insolation at 65°N (Berger, 1978). This insolation is filtered using Paillard's truncation method (Paillard, 1998) with Equation 4,

Table 1
Modified Sea-Ice Switch Model Parameter Values

Parameter	Value
$V_{\max}$	1
$V_{\min}$	0.0667
α	0.4
p_0	0.18291
k	0.01750
$\bar{a}_{si}$	0.36
S_0	0.09473
S_M	0.25265

$$f(x) = \frac{1}{2}\left(x + \sqrt{4a^2 + x^2}\right). \quad (4)$$

With $a = 1$ and x representing the insolation standardized by dividing by its standard deviation, this filtering damps negative insolation anomalies, accounting for a weaker effect of negative insolation anomalies on ablation than positive anomalies. We then re-scale $I_{\text{trunc}}(t)$ to be between 0 and 1.

We modify the SIS model to adjust the conditions determining when sea ice (the a_{si} parameter) is turned on or off, via a parameter α introduced as follows. Consider the SIS mechanism, starting from a point with low ice volume and no sea ice. The accumulation rate is high, and as the land ice volume grows, the growth is at first quick but slows due to the elevation desert effect. When the land ice volume increases, the induced cooling leads at some point to the growth of sea ice. An extensive sea ice cover lowers the snow accumulation over land ice significantly by reducing the moisture supply to the ice sheet by cooling the atmosphere and reducing evaporation, thus starting the deglaciation phase. We assume here that the atmospheric/upper ocean temperature affecting the formation of sea ice is influenced by both ice volume, via the albedo effect, and insolation, via a combination of the form $V - \alpha I(t)$ (which decreases with increasing insolation). Therefore, when $V - \alpha I(t)$ becomes larger than a specified threshold $V_{\max}$, the atmospheric and sea surface temperatures are assumed cold enough to induce a rapid formation of sea ice, and the nondimensional sea ice area is set to $\bar{a}_{si}$. This causes the accumulation to be less than the ablation due to the $(1 - a_{si})$ term in Equation 3. Ablation continues, and the land ice begins to retreat as net ablation exceeds net accumulation until $V - \alpha I(t)$ is smaller than a threshold $V_{\min}$. The implied climate warming would lead to the melting of sea ice, and the model, therefore, sets $a_{si} = 0$, leading to an increase in snow accumulation and the rebuilding of the ice sheet. We set the SIS model constants to the values given in Table 1. The modified SIS has 8 tunable parameters, and they were adjusted to fit the observed ice volume proxy record. We use the modified SIS given in Equation 3 to represent the self-sustained ice ages scenario.

3. Results

Our objective is to identify differences between the predictions of the two scenarios for ice age dynamics that can be tested against the observed record. We do this by examining several aspects of the results of each scenario: (a) how well it fits the observed proxy record time series, (b) how well it fits the observed power spectrum, (c) the implications of each scenario for the phase relation between Milankovitch forcing and ice age termination times, (d) is there a significant relationship between the magnitude of ice volume fall during terminations and the insolation integrated over that period, (e) sensitivity to initial conditions, and (f) sensitivity to noise.

3.1. Fit to Proxy Record and Spectrum

Starting with how well each scenario fits the observed record, Figure 2a shows the results of our simple IDSM, compared to both ice volume proxy records and the results from AO2013. The IDSM fits the results of AO2013's complex model surprisingly well for the first four terminations (solid vs. dashed blue in panel 2a). The saw-tooth shape is well captured by the IDSM, and the terminations are consistent with the proxy records for the last 400 Kyr, except for the second cycle (218–126 ka), in which the glacial maximum does not reach as high as observed, and there is a dramatic drop in ice volume during the build-up toward the maximum. The model representing this insolation-driven scenario also does not capture the record for the previous 400 Kyr well, and, in addition, the most recent termination does not reach the same minimum in ice volume. Both simple models appear to have some offsets from the observed timings of terminations which could be due to errors in the age model of the benthic stack or the inability of the simple model to capture all of the complexities of glacial cycles. This is further explored in Figure 3. A notable difference between the IDSM and observations occurs at T5 (419 ka), which is missed by the IDSM. This "missed termination," is further investigated in Figure 4.

Figure 2b shows the time series for the self-sustained scenario as represented by the modified SIS. The modified SIS model also does not always capture the precise volume of the proxy record. Specifically, the SIS reaches a much higher land ice volume during a glacial maximum than is seen in the proxy record of Marine Isotope Stage 8

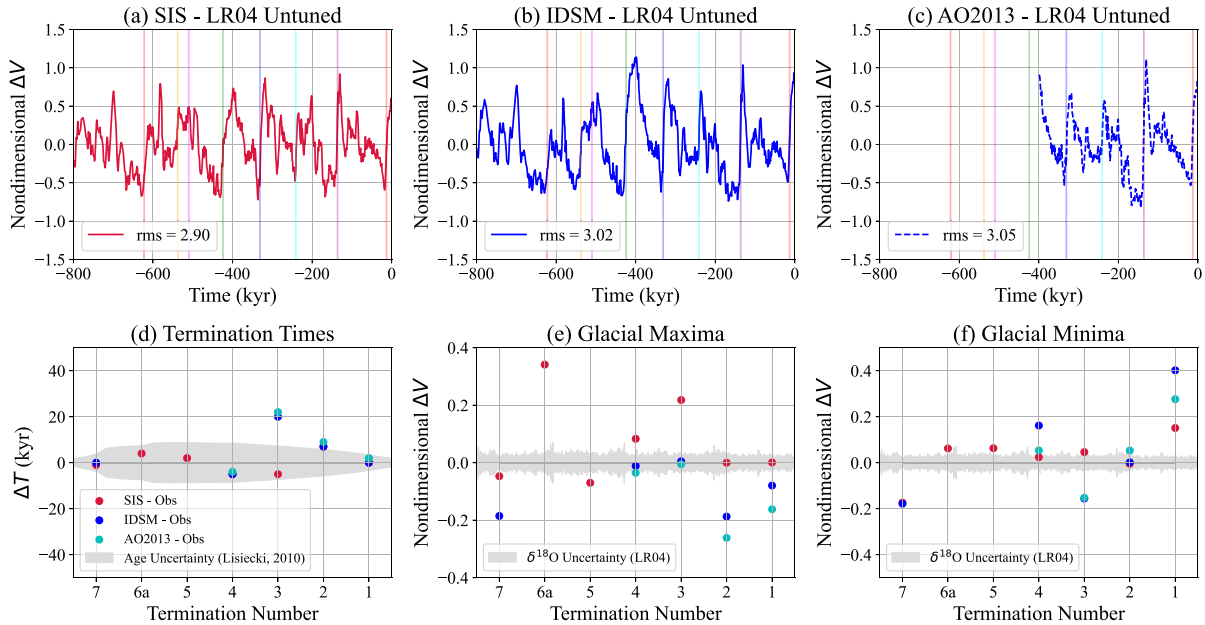

Figure 3. Quantifying the fit to observations. (a) The SIS's ice volume values minus observations with the mean (−2.88) removed. The colored vertical lines indicate the timings of the midpoints of ice volume during each termination. (b) and (c) are the same as panel (a) but for the IDSM (mean of −2.99) and AO2013 (mean of −3.02). (d) Scatter plot of the time of the midpoints of each termination minus the mid-point termination time from observations. Red marks sea ice switch (SIS), blue IDSM, and cyan AO2013. The gray region indicates the uncertainty range as calculated and shown in Figure S1 in Supporting Information S1 of Lisiecki (2010). Note that the second and first termination of the SIS are overlapping with the IDSM. All but T2 of the SIS fall within the 1 standard deviation error range of observations, whereas both the third and second of the IDSM do not fall within the range. The SIS has an root mean square (RMS) of 4.14, IDSM 9.74, and AO2013 12.09. Model-proxy differences in ice volume for each termination are shown for glacial ice volume maxima (e) and minima (f). The gray range is the standard error of the benthic δ^{18}O stack of Lisiecki and Raymo (2005). For glacial maxima, the SIS has an RMS of 0.16, IDSM 0.12, and AO2013 0.15. For glacial minima, the SIS has an RMS of 0.10, IDSM 0.22, and AO2013 0.16.

and 13 (248 and 540 ka). Despite this, it nicely depicts the overall trends in the records, especially the timings of terminations over the entire time period. Interestingly, the modified SIS does show a two-stepped termination for T6 similar to (with different magnitude) that shown in the observations (540–496 ka). We consider only the second step a termination and ignore the first, which is smaller in this model.

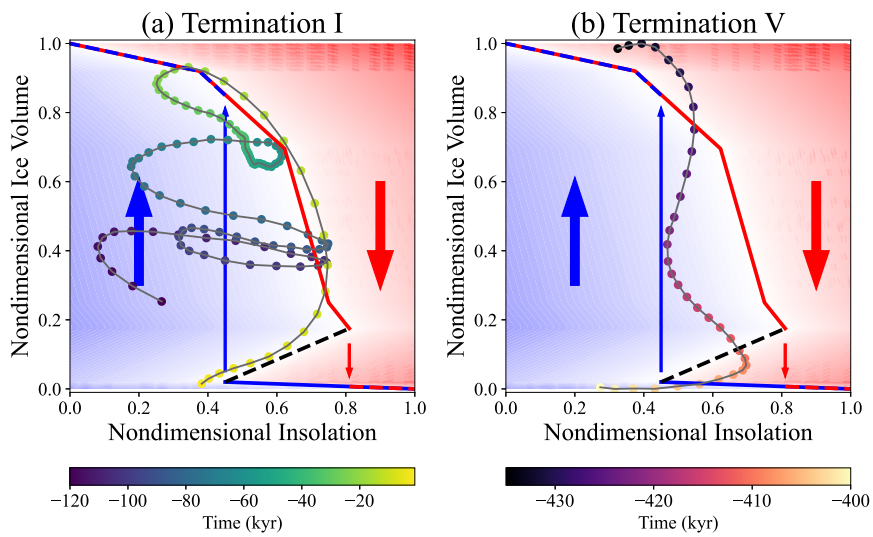

Figure 4. Ice volume versus insolation: (Plot format follows AO2013) The curves describe the ice volume trajectory with the dots spaced every 1 Kyr and increasing time indicated with the dots changing color from purple to yellow. (a) Smoothed proxy records for the last 120 Kyr (T1) and (b) smoothed proxy records for T5 (between 450 and 380 ka).

To quantify the fit of the models examined here, we use three diagnostics. First, we plot a time series difference (model ice volume values minus observations) in Figures 3a–3c. The shown time series are with the means removed and with the root mean square (RMS) value indicated. It seems that the self-sustained scenario fit is slightly better based on the RMS value of 2.90 compared to the IDSM's 3.02, although the difference is quite small. Next, we calculate the times of the midpoints of each termination in the models and subtract the midpoints times of the observations (Figure 3d). The SIS termination times (RMS value of 4.14) are much closer to the observed than the IDSM (RMS value of 9.74). Note that we used T6a as the "truth" for this analysis as Spratt and Lisiecki (2016) suggested that the majority of ice volume change happens during this termination. Specifically, the first two terminations of both simple models compare well to observations. The IDSM's T3 and T5 differ by ∼20 and 10 Kyr from observed, whereas the SIS deviates by around 5 Kyr, and all terminations except for T2, fall within the age uncertainty range of the observations (Lisiecki, 2010).

In Figure 3e, the nondimensional ice volume for each glacial maximum is plotted, showing that the SIS mostly overestimates land ice volume extent and the IDSM mostly underestimates it. Based on the RMS values, the SIS and IDSM approximate glacial maximum extent to the same level though the IDSM does slightly better (RMS of 0.12 compared to 0.16 of the SIS). Finally, Figure 3f shows the ice volume for each glacial minimum. In this, the SIS estimates ice volume minima somewhat better than the IDSM based on the RMS values (RMS of 0.1 compared to 0.22).

A comparison between the most recent glacial cycle of the last 120 Kyr and T5 (450–380 ka) is plotted in Figure 4 following the visualization approach of AO2013. The figure shows a blue region on the left side of the hysteresis loop and a red region on the right side, corresponding to positive and negative ice volume rates of change, respectively, as calculated using Equation 1. In the red regions, an initial ice volume for a given fixed insolation is expected to decrease, as indicated by the red arrows. Similarly, an initial ice volume in the blue regions will grow, as indicated by the blue arrows. Also shown in this figure is a black dashed line which is the hysteresis' unstable branch. The colored dots connected by a gray curve correspond to the observed ice volume trajectory as a function of insolation.

In panel 4a, the observed ice volume (smoothed) depicted by the purple to green dots (representing 120–20 ka) mostly grows in the blue positive mass balance regime, as expected by a dynamic governed by this hysteresis shape. Then the ice volume mostly decays in the red negative mass balance regime shown by the green to yellow dots (20–0 ka), again as expected. However, panel 4b shows that during T5, which is not simulated correctly by the IDSM, the ice volume decreases when in the blue positive mass balance regime. This suggests that this termination is inconsistent with the idea that ice ages are due to insolation driving this hysteresis. This analysis was not possible to perform in AO2013 where the mass balance was indicated on their similar plot only schematically and not inside the hysteresis loop, and where the unstable branch and its effect on the mass balance inside the hysteresis loop was not noted.

Figure 5 shows a log-log plot of the power spectral densities (PSD) of observations (Figure 5a), SIS (Figure 5b), IDSM (Figure 5c) using the last 800 Kyr. Figure 5d shows the PSD of the last 400 Kyr of the results of AO2013. The spectrum of the SIS nicely replicates the 100-Kyr peak in observations, whereas the IDSM's 100-Kyr peak is not as dominant as in the observations nor in comparison to the other spectral peaks at 40 and 20 Kyr. In fact, the IDSM has a low-frequency 400-Kyr peak which is not seen for the proxy record reconstruction of LR04 untuned. Note that the robustness of a 400 Kyr peak is not known, given the length of the time series is only 800 Kyr. However, an artificial 400 Kyr peak is a well-known issue with many insolation-driven theories (Imbrie & Imbrie, 1980; Paillard, 2001).

3.2. Phase Between Ice Age Termination Times and Milankovitch Forcing

The mechanism by which Milankovitch forcing affects the time of terminations is different for the two scenarios we are considering. In the case of insolation-driven ice ages, a large summer insolation value due to Milankovitch variations simply pushes the ice sheets into a negative mass balance (red region in Figure 1), leading to a termination. In the self-sustained scenario, the relation is more refined: a gradual weak nudging toward a certain phase over the entire cycle leads to a certain phase relation between Milankovitch forcing and ice volume, but there is no expectation that the termination is directly driven by, or occurs during the time of high insolation, necessarily. The phase relation between Milankovitch forcing and ice volume (to be defined more precisely momentarily) is, therefore, an important testable diagnostic. Raymo (1997) has

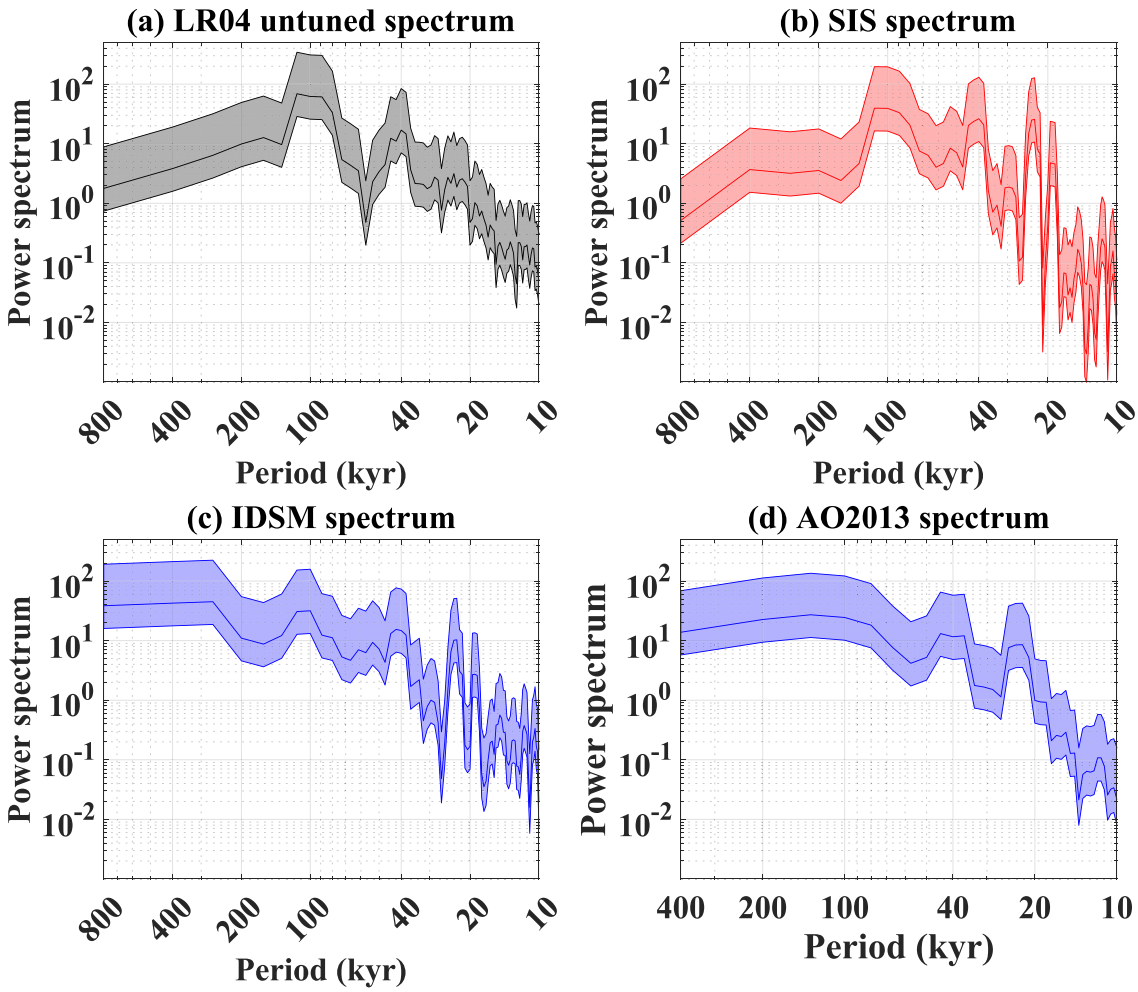

Figure 5. Log-log plots of the power spectra calculated using the multi-tapering method for the last 800 Kyrs of (a) LR04 untuned; (b) self-sustained oscillations (sea ice switch); (c) insolation-driven oscillations (IDSM); and the last 400 Kyrs of AO2013 in panel (d). The 95% confidence ranges are given by the shaded regions of each plot.

examined this issue for observations, for example, and the relation was examined for the unmodified SIS mechanism in Tziperman et al. (2006).

Figure 6 shows all the terminations for the past 800 Kyr, plotting the proxy data and the corresponding insolation (Figure 6a), obliquity (Figure 6b), and precession (Figure 6c). For the observations in Figure 6a, the timings of the peaks in insolation are different during the different terminations. To compare the phase of insolation (or obliquity or precession) during terminations, the value of the phase of insolation during the midpoint of the termination is examined. Define t_{mid} as the time of the midpoint ice volume of the termination (defined as the average of the nearby peak and minimum in ice volume). Then define t_0 to be the time of the closest maximum in insolation preceding t_{mid} and t_1 to be the time of the closest maximum after t_{mid}. Then to calculate the phase of insolation during termination, θ, we use $\theta_{\mathrm{mid}} = 2\pi(t_{\mathrm{mid}} - t_0)/(t_1 - t_0)$.

In Figure 7, all Milankovitch phases during the seven terminations are plotted on the unit circle following Huybers and Wunsch (2005). The phases of insolation for the proxy reconstruction data in Figure 7a shows a wide distribution of angles. It is unfortunately not possible to determine with certainty whether this is a result of the dynamics of ice ages and insolation variations or if this is due to errors in the age model of the δ^{18}O records. The stated error in the age model of the δ^{18}O records is approximately $\leq \pm$ 9 Kyr (Lisiecki, 2010, Figure S1 in Supporting Information S1). The average cycle length is ~23 Kyr giving an approximate error of $\leq \pm 7/9\pi$ (140°), which is a considerable range. So from a formal point of view, the data does not allow us to examine the

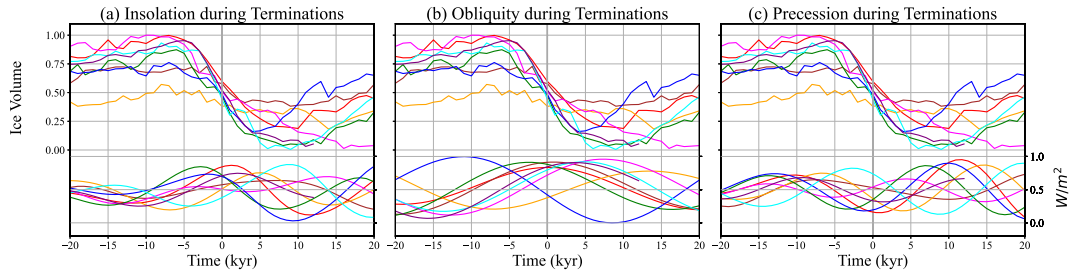

Figure 6. Phase of Milankovitch Forcing During Terminations. All the peaks of each termination are overlayed to be at time 0 on the top half of each of the plots, where the corresponding insolation measure during each termination is displayed in the lower half. (a) The LR04 untuned stack and the corresponding insolation, (b) obliquity, and (c) precession. A red color corresponds to T7, brown T6b, orange T6a, pink T5, green T4, blue T3, cyan T2, and purple corresponds to the Last Glacial Maximum or termination T1. A visual representation of the color coding used in this paper is shown in Figure 9. Note that we break T6 into two steps (termed here a and b, see also Spratt & Lisiecki, 2016), see Figure 9a for the definition of this termination. T6a (orange) reaches a smaller ice volume maximum than the other terminations making it appear misaligned.

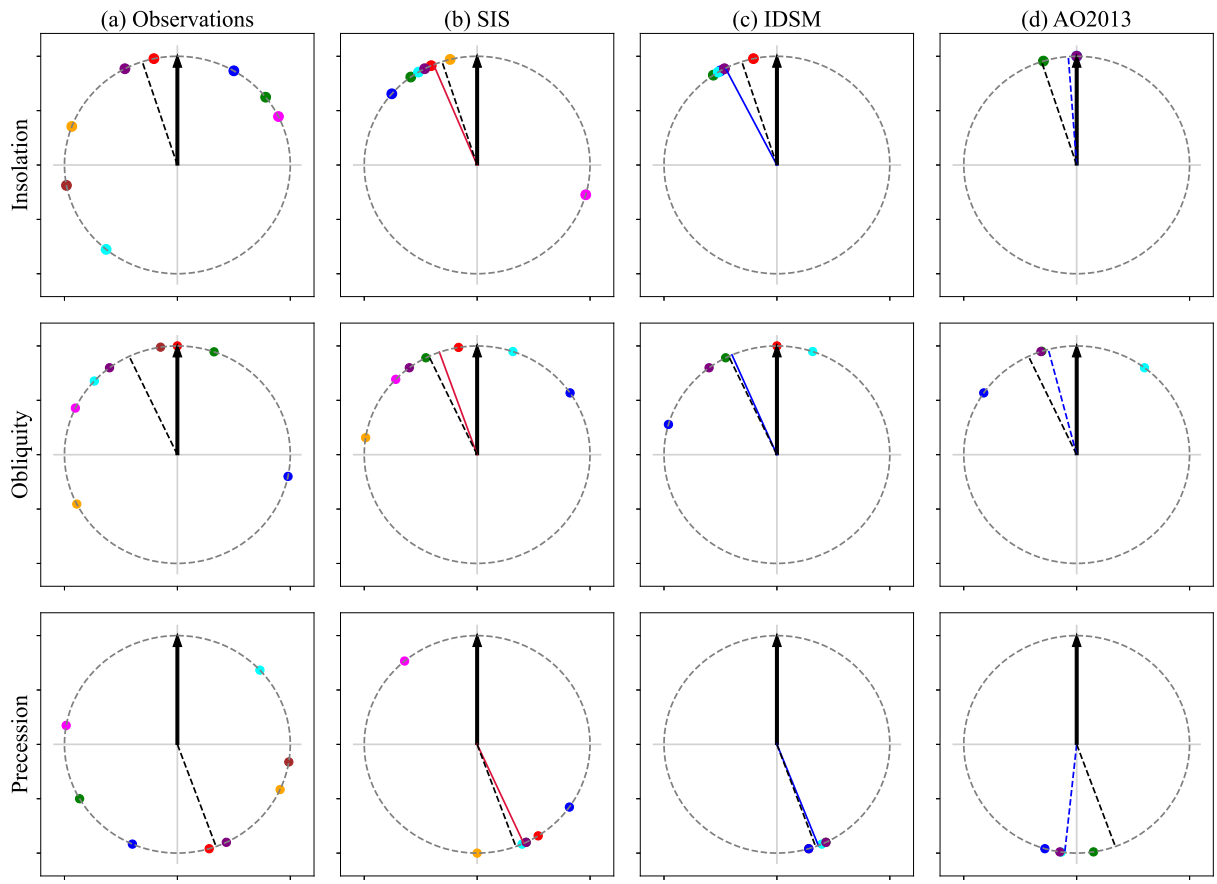

Figure 7. Plot of the phase of insolation (first row), obliquity (second row), and precession (third row) at the midpoints of terminations of observations in panel (a), the self-sustained oscillations using the modified sea ice switch (SIS) model in panel (b), insolation-driven oscillations using the IDSM model in panel (c), and finally AO2013 in panel (d). Red corresponds to T7, brown T6b, orange T6a, pink T5, green T4, blue T3, cyan T2, and purple corresponds to the Last Glacial Maximum or termination T1. A visual representation of the color coding used in this paper is shown in Figure 9. The black dashed line represents the observational circular mean of the phase of insolation, obliquity, and precession for each row. The thicker black arrow depicts the $\theta = 0$ with increasing angles clockwise around the circle. The phase of insolation for observations has a circular mean of 5.97 with a circular standard deviation of 1.32, for SIS circular mean of 5.89 and STD of 0.77, IDSM has a mean of 5.81 with a STD of 0.14, and AO2013 a mean of 6.21 with STD of 0.13. For the phase of obliquity, observations has a circular mean of 5.84, SIS 5.94, IDSM 5.87, AO2013 6.02 as well as has a STD of 1.04, 0.73, 0.56, and 0.58. Finally, for the phase of precession, observations has a circular mean of 2.79 and STD of 1.36, SIS 2.72 with 0.87 STD, IDSM 2.77 with 0.075 STD, and AO2013 has a circular mean of 3.25 with 0.16 STD.

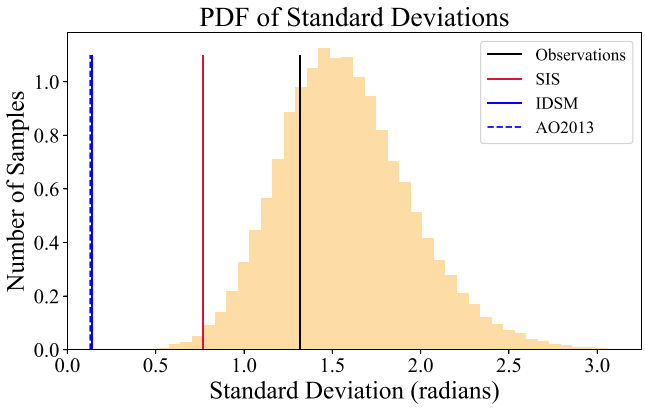

Figure 8. The probability distribution function (PDF) of the standard deviations of an ensemble set of seven randomly generated angles. The vertical lines superimposed on the PDF represent the standard deviations of the phases of insolation during terminations of each model and observations (black: observations (25.3%), red: the modified sea ice switch (0.7%), blue: the IDSM (0.0%), dashed blue: AO2013 (0.0%)). Note that the blue and dashed blue lines are overlapping.

Milankovitch phase in any meaningful way. We proceed, understanding that our discussion is subject to this caveat.

Figure 7 depicts the phase of insolation during a termination as a clock with increasing angles clockwise about the circle. A midpoint at a maximum in insolation would occur at the top point (0,1) on the circle. So, a clustering of midpoints close to 2π would imply that a minimum in ice volume corresponds to a maximum in insolation. In Figure 7c, the midpoints of terminations of the IDSM occur just before a maximum of insolation, with all of them closely clustered together. This is consistent with this model being insolation-driven, as a significant decrease in ice volume requires a maximum in insolation. The circular mean of the IDSM midpoints occurs slightly before that of observations as well. In Figure 7b, the modified SIS shows a seemingly similar clustering of phases with T5 as an outlier (although see further analysis of the std below in Figure 8). In Figure 7d for the AO2013 results, the terminations during the last 400 Kyr resemble the result of the IDSM, and the terminations again occur just before a maximum of insolation.

We have carried out a similar analysis of the phase of obliquity and precession during terminations (see second and third rows of Figure 7). The figure shows that the phases of obliquity for all models fall on one side of the unit circle. For observations, there is a wider spread of angles, but they mostly fall on one side as well. Interestingly, the pattern of terminations and the corresponding phase of obliquity for observations and the SIS are remarkably similar; however, the mean of phases for the IDSM is closer to observations. For precession, the Stage-11 problem is clearly seen by the pink dot denoting T5 being outside of the cluster for the SIS (column b), but not as clearly shown in observations (column a). As explained by AO2013, precession drives the results of AO2013, and it seems to drive also the IDSM here, as is clearly shown by the clustering of precessional phases in the IDSM and AO2013 (columns c, d). We note that our analysis examines the mid-point of terminations rather than the initiation of a termination (defined as a 2 standard deviation drop in ice volume in Huybers and Wunsch (2005) or as the local maxima as in Huybers (2011)).

To test if the Milankovitch phases during the seven terminations shown in Figure 7 are random, we follow a similar procedure to that used by Huybers and Wunsch (2005), and repeatedly sampled eight randomly generated angles between 0 and 2π. Note we include eight as T6 is broken into two steps and thus includes two phases. We then calculated the circular mean and circular standard deviation of this set. This was repeated 50,000 times to generate a histogram of the probability distribution function (PDF) of the standard deviations of each ensemble.

In Figure 8, the PDF of standard deviations of the randomly sampled phases is plotted with vertical lines corresponding to the circular standard deviation of the Milankovitch phases during terminations for observations (black), modified SIS (red), AO2013 (dashed blue), and IDSM (blue). The observation's circular standard deviation corresponds to the 25.3 percentile of the standard deviation of the distribution of random angles, implying that the observed distribution of Milankovitch phases during terminations is random within the usual 90% significance test.

The modified SIS's red line corresponds to the 0.7 percentile of the random distribution, and the IDSM and AO2013 results are effectively at the 0.0 percentile of the ensemble set of standard deviations. This analysis shows that the distributions of angles of the models representing both scenarios are not random, unlike observations. The standard deviation of the insolation-driven models is far smaller than that of the observations and of the self-sustained model. This one piece of evidence suggests that ice ages may not be insolation-driven but rather phase-locked by insolation, subject to the caveat that our analysis is based on two specific simple models, etc. The equivalent analysis for obliquity and precession are also shown to not be random for the models yet random for observations in Figure S4 in Supporting Information S1 with the percentiles listed in the supplementary material.

In summary, we find that the model used here to represent the self-sustained phase-locked scenario leads to a somewhat better fit to termination times (Figure 3), a more realistic spectral peak at 100 Kyr (Figure 5), and a weaker relation between the phase of Milankovitch forcing and termination time, again consistent with observations (Figure 7). Although no robust conclusions can be made due to age uncertainty, this analysis produces

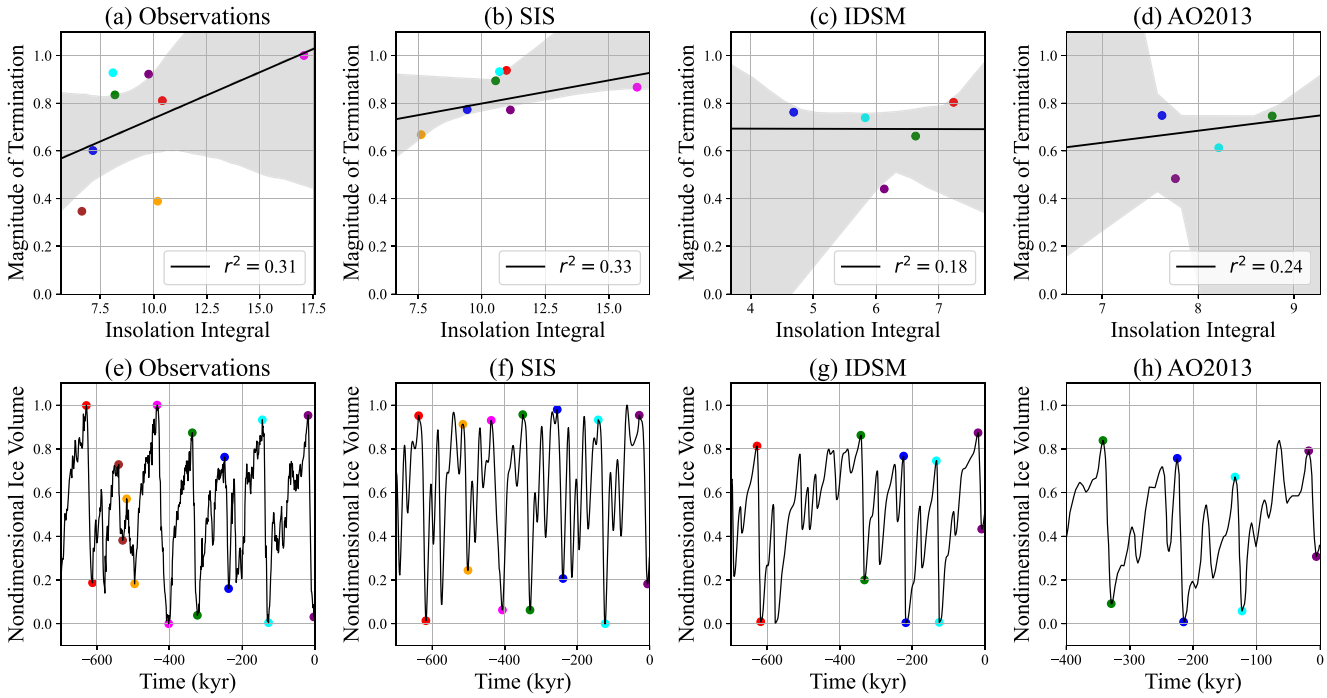

Figure 9. Plots of the ice volume drop during each termination versus insolation integrated over that same period. Observations are plotted in panel (a) with the corresponding color coding plotted below. The sea ice switch relationship is shown in panel (b), IDSM in panel (c), and AO2013 in panel (d). Shown in panels (e–h) are the time series for the observations and models with the glacial maxima and minima denoted by the colored dots marking the terminations.

observable differences between the two models, and we present this as a possible avenue of distinction if more certain, untuned stacks were to be presented and a larger class of untuned stacks were to be analyzed.

A similar analysis was performed using the orbitally tuned LR04 stack (not shown) and showed that observations and the modified SIS shared remarkable similarities. Interestingly, the results for the insolation-driven models were very different from those of the tuned observations. This further highlights the uncertainties in the analysis we attempt here due to the proxy record age model.

3.3. Ice Volume Drop During Terminations Versus Insolation Magnitude

We next compare the ice volume drop during terminations to the insolation integrated over the period of termination. On the one hand, Roe (2006) found that dV/dt can be approximated by $I(t)$ throughout time, and Mitsui et al. (2022) found that the size of terminations is directly related to the amount of insolation integrated over the caloric summer half of the year. On the other hand, one expects physical processes other than insolation to significantly contribute to the retreat of the ice sheets during terminations (e.g., sea ice shutting off snow accumulation in the SIS mechanism), so it is not obvious that there should be a relation between dV/dt and ice volume change during terminations, specifically. These two different contrasting views of the role of Milankovitch forcing during glacial terminations suggest that analyzing this relation, as done in the current subsection, may help distinguish between different model scenarios.

We calculate the drop in ice volume as the ice volume at the peak of an ice age minus the ice volume during the following minimum (see bottom row of Figure 9). This analysis tests if ice volume V changes during terminations are directly driven by Milankovitch forcing $I(t)$: integrating a schematic equation of the form $dV/dt \propto I(t)$ over the termination period, the left-hand side becomes the ice volume drop during the termination and the RHS the termination-integrated insolation over the termination period.

We then fit a line to each scatter plot and use a bootstrapping resampling technique to estimate the error bounds and statistical significance of the best-fit lines to the data. In this, we randomly sample eight times out of our eight data points (representing observed terminations) on each graph (and similarly 7 out of 7 terminations for the SIS, 5 for the IDSM, and 4 for AO2013). The slope, intercept, p-value, and r^2 value of each sampling are calculated. This

is then repeated $N = 10{,}000$ times, and a histogram of each of the four parameters is plotted as a PDF in supplementary Figure S4 in Supporting Information S1. We use these histograms to estimate the 90% confidence range for the fitted line in Figure 9 (details in supplementary information).

For observations, Figure 9a shows what appears to be a correlation between the size of ice volume drop and termination-integrated insolation. However, this involves significant uncertainty due to the large error range indicated by the gray shading, the small r^2 value of 0.31, and the ambiguity in the definition of T6. T5, depicted by the pink point, appears to be the most obvious outlier, exhibiting the Stage-11 problem. For the SIS, there appears to be a similar positive trend with a smaller uncertainty ranger and similar $r^2 = 0.33$ value (see Figure 9b). The positive correlation is a reflection of the activation of the SIS being a function of insolation in addition to the effects of nonlinear phase locking. In Figure 9c, we also see little to no correlation ($r^2 = 0.18$) between ice volume drop and termination-integrated insolation in the IDSM with a very large uncertainty bound due to the fact that we are only including five data points as the IDSM misses the fifth and sixth terminations. The large uncertainty range in Figure 9c also comes from the fact that even in an insolation-driven scenario, as represented by our IDSM, the volume rate of change during termination is not determined only by the variations in insolation but is strongly affected by the piece-wise linear RHS (see Equation 1 and Figure 1), which encodes different feedbacks.

In summary, there is no statistically significant relationship between the size of ice volume fall and termination-integrated insolation for the observations, nor for any of the models, and we further discuss this in the conclusions section. This analysis suggests that one cannot use this measure to distinguish between internally- or insolation-driven glacial cycles. Note that this result is affected by our analysis choices, such as defining T6 to include two steps, the choice of insolation measure as opposed to other possibilities (e.g., caloric summer half-year insolation, Mitsui et al., 2022), etc.

3.4. Sensitivity to Initial Conditions

In both scenarios considered here, Milankovitch forcing sets the time of glacial inceptions and terminations. We wish to study this aspect in detail and identify any testable differences between the way this occurs in the two scenarios. One way to do so is to study the sensitivity of the model results to its initial conditions (i.e., the initial ice volume). To investigate the dependence of each model on the choice of initial conditions, we start with 10 initial conditions for the nondimensional ice volume, uniformly spread over 0 to 1, and plot the resulting time series. We repeat with such an ensemble of initial conditions prescribed at different starting times (900, 700, 500 ka). These results are seen in Figure 10.

AO2013 explained that their results are not sensitive to initial conditions beyond some adjustment period, and we find the same to be true for the IDSM, which reproduces their mechanism (Figure 10a). In the IDSM, the paths starting from different initial conditions quickly converge after a short adjustment period of up to 20 Kyr, with occasional initial conditions taking up to 80 Kyr to adjust (Figure 10a). This results from the insolation variations directly affecting ice volume as it is forced through the hysteresis loop. As explained in AO2013, when the ice volume is large, a strong Milankovitch forcing puts it in the negative surface mass balance regime and leads to a rapid decrease of the ice volume and to a termination. This direct relation between Milankovitch forcing and terminations leads to the convergence of different initial conditions to the same path.

In the modified SIS model (Figure 10b), the runs using different initial conditions eventually converge to two distinct trajectories. The convergence occurs after less than 100 Kyr, but still over a longer adjustment period than in the IDSM. Such a convergence is a characteristic of a nonlinear phase locking between the self-sustained oscillations of glacial cycles and the Milankovitch forcing (Crucifix, 2013; Gildor & Tziperman, 2000; Hyde & Peltier, 1987; Tziperman et al., 2006). "Phase locking," or "nonlinear resonance," refers to the synchronization of a nonlinear oscillator to a periodic forcing (or to another nonlinear oscillator). For strict phase locking to occur in the sense used, for example, by Pikovsky et al. (2001), the existence of unforced, self-sustained oscillations is required. When the forcing is perfectly periodic, the locking occurs such that the oscillation frequency ω, and the forcing frequency Ω satisfy $\omega/\Omega = p/q$ with p, q integers (Pikovsky et al., 2001; Strogatz, 1994). Phase locking occurs by the periodic forcing applying weak nudging throughout the cycle toward a certain phase. In the two scenarios of glacial cycles considered here, only the scenario involving ice ages as self-sustained oscillations can be considered as phase-locked to Milankovitch cycles.

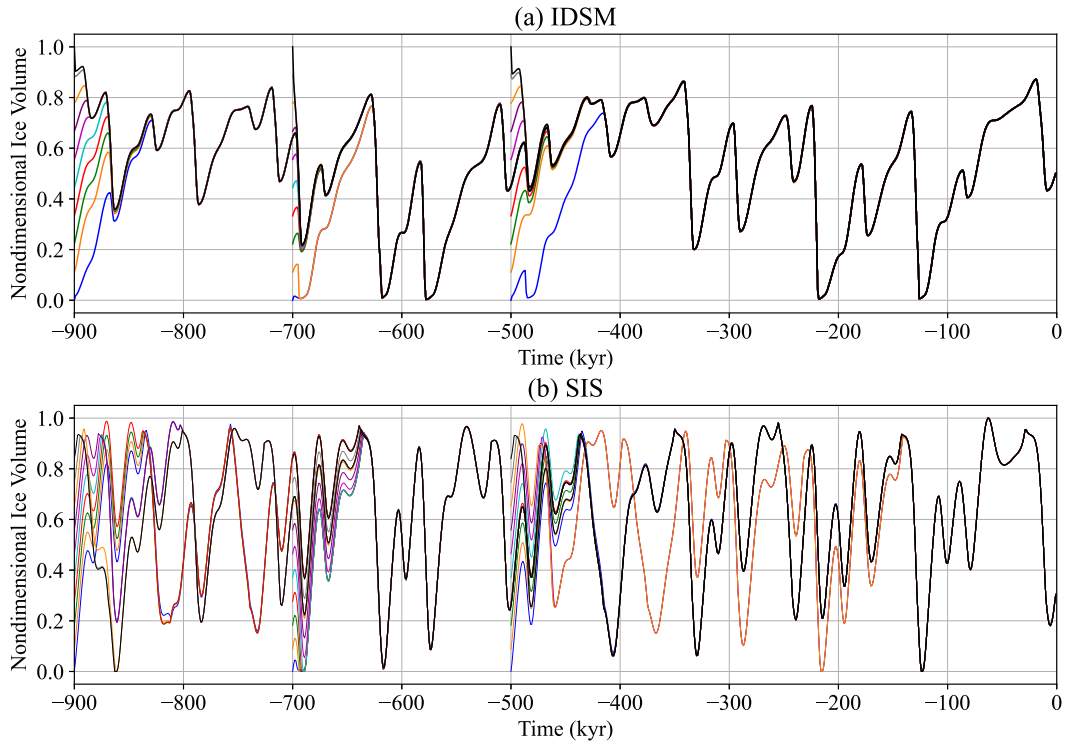

Figure 10. Plot of the dependence of initial conditions for the IDSM (a) and the modified sea ice switch (b). Each color represents a different initial condition and is the same in both (a, b).

To see why two paths of ice volume as a function of time might emerge from the many different initial conditions in Figure 10, consider an idealized Milankovitch forcing (a pure sine wave) with a period of 40 Kyr and a glacial cycle that locks into an 80 Kyr period (see Figure 1c in Tziperman et al. (2006)). Because the model is phase locked at $p/q = 1/2$, the model time series can adjust such that terminations happen either at t_0, $t_0 + 80$, $t_0 + 160\ldots$ or at $t_0 + 40$, $t_0 + 120$, $t_0 + 200\ldots$ where t_0 is the relevant initial start time. The non-uniqueness of the phase locking occurs due to the shift in the forcing time series by 40 Kyrs that produces the exact same forcing.

The results of Figure 10 suggest an important way of differentiating between the self-sustained and insolation-driven ice age scenarios. In the first, different initial conditions lead to a unique ice volume time series, while in the second, different phase-locked time series are possible. This does not lead to an observable difference using the proxy record. Yet, using this test of different initial conditions with a realistic climate model can help us understand what scenario applies in that model, and, in turn, in the climate system as well. Of course, current state-of-the-art climate models that can be run over multiple glacial cycles are limited in their ability to include accurate representations of the most basic climate processes and thus, in their ability to provide information about the real climate system.

3.5. Effects of Noise

Climate variability ranges from long timescales, such as glacial cycles, to shorter timescales that can be treated as "noise" or stochastic forcing in the context of glacial cycles. We are interested in the effects of such noise on the two scenarios studied here. To investigate such effects, we run the model $N = 200$ times for each noise amplitude (see Equation 2) and with different realizations of noise. For each such run, we calculate the deviation from the no-noise case (averaged sum of squares, at a resolution of 1 Kyr), and then the mean (over noise realizations) deviation for each noise level. Figure 11b, shows that for some noise realizations, at a noise amplitude of 0.01, the modified SIS jumps to a different path altogether rather than slightly deviating from the original path. This is evidence of the modified SIS model phase locking to a different path due to the periodicity of the precession forcing (Tziperman et al., 2006), consistent with the results of the previous subsection. Figure 11a shows that the locking of the insolation-driven case, as represented by the IDSM to Milankovitch, is much more robust to noise.

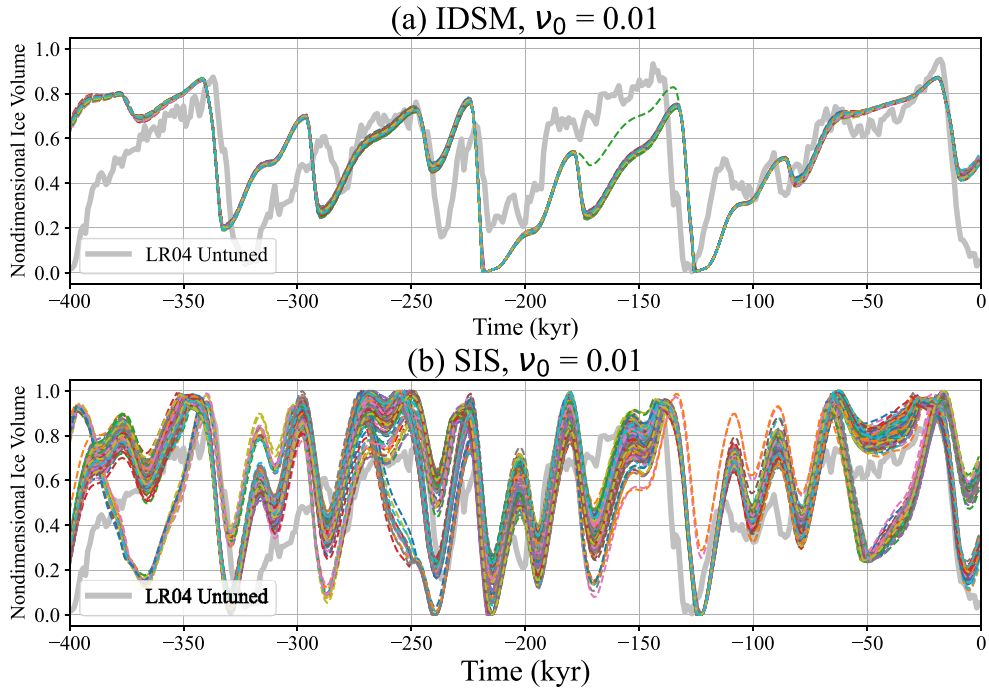

Figure 11. Ice volume time series from 200 runs for a noise amplitude of $\nu_0 = 0.01$. (a) The ensemble for the IDSM in the colored dashed lines. (b) The same, for the sea ice switch.

The noise merely broadens the ice volume time series, except in one case between 180 and 130 ka, where a second path emerges briefly. This is again consistent with the robustness of the IDSM to different initial conditions seen in the previous subsection.

To test the sensitivity to different noise amplitudes, we repeat the same analysis for ten different noise amplitudes in the range of 0–0.09. We plotted the mean deviation as a function of the noise amplitude with a shaded region corresponding to 1 standard deviation spread around the mean value at each noise level. These results are plotted in Figure 12. In this, we see the general increase in difference from a no-noise run for both the SIS and the IDSM, although the SIS is clearly much more sensitive to an increase in noise amplitude.

The larger sensitivity of the self-sustained phase-locked (SIS) scenario to noise can be explained as follows. Increasing the noise amplitude slightly smears the IDSM, yet it occasionally causes the SIS to take completely different ice volume paths that are still consistent with phase locking to Milankovitch forcing. Such different paths are expressed as a large deviation from the no-noise solution, as seen in the difference from the no noise run shown in Figure 12. The lower sensitivity to noise of the IDSM is an expected feature of insolation-driven models: in phase-locked models insolation only weakly affects the mass balance, allowing a more dominant role for stochastic forcing. Yet in insolation-driven models, the mass balance is dominated by the effects of insolation, making the effects of stochastic forcing less dominant.

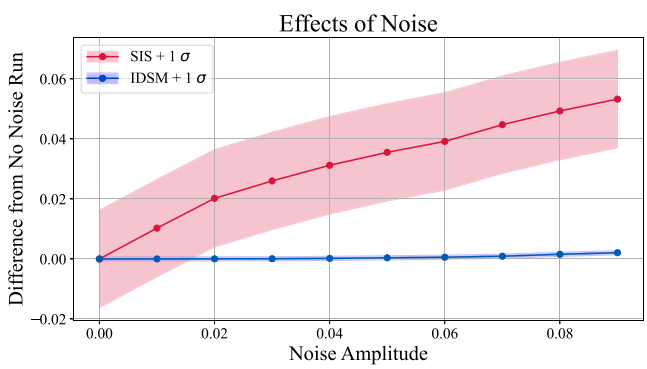

Figure 12. The effects of noise on the two scenarios. The deviation of the model time series from the no-noise case for the modified sea ice switch mechanism is given by the red line. The equivalent result for the insolation-driven simple model (IDSM) is given by the blue line. The shading represents a range of ±1 standard deviation.

We conclude that the phase-locked mechanism is more sensitive to noise for the two models considered here, but likely more generally due to the more fundamental role Milankovitch variations play in the insolation-driven scenario. To be relevant, the self-sustained scenario must be robust to reasonable amplitudes of noise so that termination times are consistent with the observed record. However, given a different noise realization due to different internal climatic variability, *if* ice ages are represented by a self-sustained oscillation like the SIS, then we might have seen different timings of the records if ice

ages were phase-locked. As in the sensitivity to initial conditions discussed above, this does not lead to an observable difference between the two scenarios but helps our understanding of the implications of the two.

4. Conclusions

Over the past 800,000 years, Earth's climate has been dominated by the wax and wane of massive Northern Hemispheric glacial oscillation with an approximate 100,000-year periodicity. Although it is clear that Milankovitch insolation variations played a role in these cycles, the exact influence of these variations on the evolution of ice sheets is still to be resolved, and we considered two scenarios. In one, the effect of Milankovitch variations is driving the cycles, which would not have existed without these variations. In the second, Milankovitch variations only set the phase of the oscillation (e.g., the timing of terminations), but the glacial oscillation is self-sustained and would have existed even without Milankovitch changes.

To develop methods that may allow us to figure out which scenario is more relevant to the observed ice ages, we examined two different glacial models corresponding to these two possibilities. First, representing the insolation-driven glacial cycle mechanism, we developed a simple model (the IDSM) based on the work of Abe-Ouchi et al. (2013, AO2013). Second, representing the self-sustained glacial cycle mechanism, we used a modified version of the SIS model (Gildor & Tziperman, 2000; Tziperman et al., 2006). The modified SIS was tuned to fit observations whereas the IDSM was tuned to fit the work of AO2013 in order to allow testing their proposed mechanism. Our interest is not in these two particular models but in them representing the two different roles of insolation variations.

We developed and used six tests to produce observable differences between the two scenarios. First, we found that the ice volume time series of the self-sustained glacial cycle mechanism was a better fit to the proxy record than that of the insolation-driven (Figure 2). The second test examined the PSD of the proxy record and the two scenarios (Figure 5). The self-sustained glacial oscillations produced a dominant 100 Kyr peak similar to observations. The insolation-driven model produced a 100-Kyr peak; however, an additional dominant 400-Kyr spectral peak emerged–inconsistent with observations and a well-known problem of insolation-driven models (Imbrie, Berger, et al., 1993; Paillard, 2001). Our third attempt at an observable difference between the two scenarios diagnoses the phase of Milankovitch cycles during ice terminations (Figures 7 and 8). We find that the midpoint of ice volume during terminations for observations occurs over a wide range of Milankovitch forcing phases.

We find both scenarios lead to a strong clustering of the phases, more than observations. In that sense, both are inconsistent with the observed record, although the insolation-driven results are significantly more clustered, showing a much stronger phase relation between termination time and Milankovitch variations than the self-sustained oscillations or observations. We emphasize that age model errors imply that no robust conclusion can be drawn from this analysis.

Our fourth analysis examines the relationship between the size of deglaciation events and the insolation integrated over this period (Figure 9). Naively one often assumes that, at least in the insolation-driven case, a stronger summer insolation should lead to a larger ice volume loss. This is supported by the finding that the ice volume rate of change (Roe, 2006) and magnitude of termination (Mitsui et al., 2022; Tzedakis et al., 2017) are correlated with different insolation measures. However, we find that there is no statistically significant correlation between the size of the ice volume drop and the termination-integrated insolation in the observed proxy record or in the models examined. Specifically, in either scenario, while the insolation plays a role, there are other terms (piece-wise linear RHS (Figure 1) in the IDSM and the SIS dynamics), which dominate deglaciation events. It seems that this fourth analysis cannot distinguish in which scenario glacial cycles fall, but rather points to the importance of internal feedbacks in determining the shape of ice ages.

Finally, we tested two diagnostics that can be used to separate the two scenarios in models but are not directly observable: the sensitivity to initial conditions and to noise forcing of each of the two scenarios (Figures 10 and 12). These diagnostics showed that the insolation-driven model (IDSM) loses memory of initial conditions quickly and, as a result, is also very robust to noise. For the modified SIS, we show the emergence of (at least) two possible ice volume trajectories (time series) due to phase locking of the self-sustained glacial cycles to Milankovitch variations. Because noise can trigger a switch to an alternative phase-locked trajectory, the SIS is more sensitive to noise than the IDSM. This implies that *if* ice ages were self-sustained oscillations, we could have

seen different termination times than observed based on different initial conditions and noise realization in the climate system.

Our reading of these results is that, for the two example models considered here and with significant caveats to be mentioned shortly, the above observable differences seem to suggest that the self-sustained scenario is more consistent with the observed record than the insolation-driven case. This includes the time series fit and the power spectrum. The self-sustained scenario produces all terminations whereas the insolation-driven case misses T5. Yet the means of the insolation phases during terminations are comparable in both scenarios, and these means seem to be consistent with observations. However, the self-sustained scenario shows a wider spread of phases due to the phase for T5, whereas the insolation-driven case shows a strong clustering, having missed this termination. Neither scenario replicated the results of the observations sufficiently well when it comes to some of these tests. A broad class of models in each category is required to test these conclusions more robustly.

There are multiple caveats to note. We use $\delta^{18}O$ as a proxy for ice volume, neglecting the fact that a significant part of the signal reflects deep ocean temperatures (Adkins & Schrag, 2001; Spratt & Lisiecki, 2016). The uncertainty in the dating of the records results in large errors in our analysis, significantly limiting our ability to produce conclusive results. Our analysis completely relies on the two specific simple models; while some of the analyses seem to suggest robust results of more general validity, they would need to be tested with a broader set of models in each scenario. Our work omits multiple potentially important factors and feedbacks, including, for example, southern hemispheric interactions (Denton et al., 2010; Wolff et al., 2009) and millennial-scale feedbacks (Barker & Knorr, 2021) that have both been suggested to play an important role in terminations. Regardless, we feel that understanding whether ice ages are insolation-driven or self-sustained is a goal worthy of further study.

Data Availability Statement

Python files for the simple models used and explained in this paper can be retrieved from Koepnick (2024).

Acknowledgments
We thank Lorraine Lisiecki, Peter Huybers, and two anonymous reviewers for their most helpful suggestions. This work was funded by NSF Grant 2303486 from the P4CLIMATE program. ET thanks the Weizmann Institute for its hospitality during parts of this work.

References

Abe-Ouchi, A., Saito, F., Kawamura, K., Raymo, M. E., Okuno, J., Takahashi, K., & Blatter, H. (2013). Insolation-driven 100,000-year glacial cycles and hysteresis of ice-sheet volume. *Nature*, *500*(7461), 190–193. https://doi.org/10.1038/nature12374

Abe-Ouchi, A., Segawa, T., & Saito, F. (2007). Climatic conditions for modelling the northern hemisphere ice sheets throughout the ice age cycle. *Climate of the Past*, *3*(3), 423–438. https://doi.org/10.5194/cp-3-423-2007

Adkins, J. F., & Schrag, D. P. (2001). Pore fluid constraints on deep ocean temperature and salinity during the last glacial maximum. *Geophysical Research Letters*, *28*(5), 771–774. https://doi.org/10.1029/2000gl011597

Barker, S., & Knorr, G. (2021). Millennial scale feedbacks determine the shape and rapidity of glacial termination. *Nature Communications*, *12*(1), 2273. https://doi.org/10.1038/s41467-021-22388-6

Berger, A. (1978). Long-term variations of daily insolation and Quaternary climate changes. *Journal of the Atmospheric Sciences*, *35*(12), 2362–2367. https://doi.org/10.1175/1520-0469(1978)035<2362:ltvodi>2.0.co;2

Berger, A., & Loutre, M. F. (1991). Insolation values for the climate of the last 10 million years. *Quaternary Science Reviews*, *10*(4), 297–317. https://doi.org/10.1016/0277-3791(91)90033-q

Broecker, W. S., & van Donk, J. (1970). Insolation changes, ice volumes, and the O18 record in deep-sea cores. *Reviews of Geophysics*, *8*(1), 169–198. https://doi.org/10.1029/RG008i001p00169

Crucifix, M. (2013). Why could ice ages be unpredictable? *Climate of the Past*, *9*(5), 2253–2267. https://doi.org/10.5194/cp-9-2253-2013

Denton, G. H., Anderson, R. F., Toggweiler, J. R., Edwards, R. L., Schaefer, J. M., & Putnam, A. E. (2010). The last glacial termination. *Science*, *328*(5986), 1652–1656. https://doi.org/10.1126/science.1184119

De Saedeleer, B., Crucifix, M., & Wieczorek, S. (2013). Is the astronomical forcing a reliable and unique pacemaker for climate? A conceptual model study. *Climate Dynamics*, *40*(1), 273–294. https://doi.org/10.1007/s00382-012-1316-1

Donald, B., & Percival, A. T. W. (1993). *Spectral analysis for physical applications: Multitaper and conventional univariate techniques*. Cambridge University Press.

Emiliani, C. (1955). Pleistocene temperatures. *The Journal of Geology*, *63*(6), 538–575. https://doi.org/10.1086/626295

Epstein, S., Buchsbaum, S., Lowenstein, H., & Urey, H. (1953). Revised carbonate-water isotopic temperature scale. *The Geological Society of America Bulletin*, *64*(11), 1315–1326. https://doi.org/10.1130/0016-7606(1953)64[1315:rcits]2.0.co;2

Ganopolski, A., & Brovkin, V. (2017). Simulation of climate, ice sheets and CO_2 evolution during the last four glacial cycles with an earth system model of intermediate complexity. *Climate of the Past*, *13*(12), 1695–1716. https://doi.org/10.5194/cp-13-1695-2017

Ghil, M., & Saltzman, B. (1984). Oscillator models of climate change. In A. Berger, J. Imbrie, J. Hays, G. Kukla, & B. Saltzman (Eds.), *Milankovitch and climate: Understanding the response to orbital forcing* (pp. 859–866). D. Reidel.

Gildor, H., & Tziperman, E. (2000). Sea ice as the glacial cycles climate switch: Role of seasonal and orbital forcing. *Paleoceanography*, *15*(6), 605–615. https://doi.org/10.1029/1999pa000461

Hays, J. D., Imbrie, J., & Shackleton, N. J. (1976). Variations in the earth's orbit: Pacemakers of the ice ages. *Science*, *194*(4270), 1121–1132. https://doi.org/10.1126/science.194.4270.1121

Huybers, P. (2006). Early Pleistocene glacial cycles and the integrated summer insolation forcing. *Science*, *313*(5786), 508–511. https://doi.org/10.1126/science.1125249

Huybers, P. (2011). Combined obliquity and precession pacing of late pleistocene deglaciations. *Nature*, *480*(7376), 229–232. https://doi.org/10.1038/nature10626

Huybers, P. (2022). Putting the significance of spectral peaks on the level: Implications for the 1470-yr peak in Greenland δ^{18}O. *Journal of Climate*, *35*(13), 4147–4155. https://doi.org/10.1175/JCLI-D-22-0011.1

Huybers, P., & Wunsch, C. (2005). Obliquity pacing of the late Pleistocene glacial terminations. *Nature*, *434*(7032), 491–494. https://doi.org/10.1038/nature03401

Hyde, W. T., & Peltier, W. R. (1987). Sensitivity experiments with a model of the ice-age cycle: The response to milankovitch forcing. *Journal of the Atmospheric Sciences*, *44*(10), 1351–1374. https://doi.org/10.1175/1520-0469(1987)044<1351:sewamo>2.0.co;2

Imbrie, J., Berger, A., Boyle, E. A., Clemens, S. C., Duffy, A., Howard, W. R., et al. (1993). On the structure and origin of major glaciation cycles 2. The 100,000–year cycle. *Paleoceanography*, *8*(6), 699–735. https://doi.org/10.1029/93pa02751

Imbrie, J., & Imbrie, J. Z. (1980). Modelling the climatic response to orbital variations. *Science*, *207*(4434), 943–953. https://doi.org/10.1126/science.207.4434.943

Imbrie, J., Mix, A., & Martinson, D. (1993). Milankovitch theory viewed from devils hole. *Nature*, *363*(6429), 531–533. https://doi.org/10.1038/363531a0

K-1 model developers. (2004). *K-1 coupled GCM (MIROC) description, K-1 technical report No. 1 (Tech. Rep.)*. Center for Climate System Research, University of Tokyo, Japan, National Institute for Environmental Studies, and Frontier Research Center for Global Change.

Koepnick, K. (2024). kirstinkoepnick/ice-ages: v1.0.0 (v0.0.0) [Software]. *Zenodo*. https://doi.org/10.5281/zenodo.10456153

Lisiecki, L. E. (2010). Links between eccentricity forcing and the 100,000-year glacial cycle. *Nature Geoscience*, *3*(5), 349–352. https://doi.org/10.1038/ngeo828

Lisiecki, L. E., & Raymo, M. E. (2005). A Pliocene-Pleistocene stack of 57 globally distributed benthic delta O-18 records. *Paleoceanography*, *20*(1). https://doi.org/10.1029/2004pa001071

Maasch, K., & Saltzman, B. (1990). A low-order dynamical model of global climatic variability over the full Pleistocene. *Journal of Geophysical Research*, *95*(D2), 1955–1963. https://doi.org/10.1029/jd095id02p01955

Mitsui, T., Tzedakis, P. C., & Wolff, E. W. (2022). Insolation evolution and ice volume legacies determine interglacial and glacial intensity. *Climate of the Past*, *18*(9), 1983–1996. https://doi.org/10.5194/cp-18-1983-2022

Paillard, D. (1998). The timing of Pleistocene glaciations from a simple multiple-state climate model. *Nature*, *391*(6665), 378–381. https://doi.org/10.1038/34891

Paillard, D. (2001). Glacial cycles: Toward a new paradigm. *Reviews of Geophysics*, *39*(3), 325–346. https://doi.org/10.1029/2000rg000091

Pikovsky, A., Rosenblum, M., & Kurths, J. (2001). *Synchronization: A universal concept in nonlinear science*. Nonlinear Science Series 12. Cambridge University Press.

Pollard, D. (1982). A simple ice sheet model yields realistic 100 kyr glacial cycles. *Nature*, *296*(5855), 334–338. https://doi.org/10.1038/296334a0

Raymo, M. E. (1997). The timing of major terminations. *Paleoceanography*, *12*(4), 577–585. https://doi.org/10.1029/97pa01169

Roe, G. (2006). In defense of milankovitch. *Geophysical Research Letters*, *33*(24). https://doi.org/10.1029/2006GL027817

Rohatgi, A. (2022). Webplotdigitizer. Retrieved from https://github.com/ankitrohatgi/WebPlotDigitizer

Shackleton, N. (1967). Oxygen isotope analyses and pleistocene temperatures re-assessed. *Nature*, *215*(5096), 15–17. https://doi.org/10.1038/215015a0

Spratt, R. M., & Lisiecki, L. E. (2016). A late pleistocene sea level stack. *Climate of the Past*, *12*(4), 1079–1092. https://doi.org/10.5194/cp-12-1079-2016

Strogatz, S. (1994). *Nonlinear dynamics and chaos*. Westview Press.

Thomson, D. (1982). Spectrum estimation and harmonic analysis. *Proceedings of the IEEE*, *70*(9), 1055–1096. https://doi.org/10.1109/PROC.1982.12433

Tzedakis, P. C., Crucifix, M., Mitsui, T., & Wolff, E. W. (2017). A simple rule to determine which insolation cycles lead to interglacials. *Nature*, *542*(7642), 427–432. https://doi.org/10.1038/nature21364

Tziperman, E., Raymo, M., Huybers, P., & Wunsch, C. (2006). Consequences of pacing the pleistocene 100 kyr ice ages by nonlinear phase locking to milankovitch forcing. *Paleoceanography*, *21*(PA4206). https://doi.org/10.1029/2005PA001241

Weertman, J. (1976). Milankovitch solar radiation variations and ice age ice sheet sizes. *Nature*, *261*(5555), 17–20. https://doi.org/10.1038/261017a0

Willeit, M., Ganopolski, A., Calov, R., & Brovkin, V. (2019). Mid-Pleistocene transition in glacial cycles explained by declining CO_2 and regolith removal. *Science Advances*, *5*(4), eaav7337. https://doi.org/10.1126/sciadv.aav7337

Wolff, E. W., Fischer, H., & Röthlisberger, R. (2009). Glacial terminations as southern warmings without northern control. *Nature Geoscience*, *2*(3), 206–209. https://doi.org/10.1038/ngeo442